
Proceedings Paper:
Childerhouse, T., M'Saoubi, R., Franca, L.F.P. et al. (2023) Machining performance and wear behaviour of polycrystalline diamond and coated carbide tools during milling of titanium alloy Ti-54M. In: Hanke, S., (ed.) Wear. 24th International Conference on Wear of Materials, 16-20 Apr 2023, Banff, Canada. Elsevier BV. Article no: 204791. ISSN: 0043-1648. EISSN: 1873-2577.

https://doi.org/10.1016/j.wear.2023.204791

Wear 523 (2023) 204791

Contents lists available at ScienceDirect

Wear

journal homepage: www.elsevier.com/locate/wear

Machining performance and wear behaviour of polycrystalline diamond and coated carbide tools during milling of titanium alloy Ti-54M

Thomas Childerhouse [a,e,*], Rachid M'Saoubi [b,c], Luiz F.P. Franca [d], Pete Crawforth [e], Martin Jackson [a]

[a] Department of Materials Science and Engineering, University of Sheffield, Sir Robert Hadfield Building, Mappin Street, Sheffield, S1 3JD, UK
[b] Materials & Technology Development, Seco Tools AB, SE-73782, Fagersta, Sweden
[c] Department of Mechanical Engineering Sciences, Division of Production and Materials Engineering, Lund University, Naturvetarvägen 18, 223 62 Lund, Sweden
[d] Element Six (UK) Ltd, Global Innovation Centre, Fermi Avenue, Harwell, OX11 0QR, UK
[e] Advanced Manufacturing Research Centre with Boeing, University of Sheffield, Rotherham, S60 5TZ, UK

ARTICLE INFO

Keywords:
High speed machining
Advanced cutting tool materials
Tool wear
Titanium alloys
Surface integrity

ABSTRACT

Polycrystalline diamond (PCD) is currently under development as a new generation of cutting tool material for titanium alloy machining applications. The unrivaled high temperature hardness possessed by PCD offers the potential for higher levels of productivity compared to tungsten carbide, the current industry standard tool material, through facilitating higher cutting speeds. This study investigates the performance of various PCD tool grades during square shoulder milling of Ti-54M. The influence of PCD grain size on dominant wear mechanism has been established, revealing that a smaller, sub 1 μm, grain size offers improvements in tool life due to superior fracture toughness compared to larger grained material. For fine grained PCD, loss of tool material through a cyclic process of workpiece adhesion followed by grain pull-out was identified to be the predominant wear mechanism, contrasting the mechanical fracture dominated wear observed for the larger grained PCD grades. The influence of insert microgeometry was also investigated through honing of the cutting edge radii. An increased tendency for edge fracture was demonstrated when machining with larger radii tooling which was attributed to increased cutting forces. Finally, the study has compared the surface integrity response of the workpiece following PCD and carbide machining, revealing considerably lower levels of microstructural damage and cutting forces when machining with PCD. This highlights the potential benefits of PCD in finishing applications, whereby high speed machining can be employed to reduce the impact on component surface integrity.

1. Introduction

Compared to other metals, titanium and its alloys are notoriously difficult to machine owing to the fact that a number of their properties which give them such desirable in-service performance characteristics, such as their capability to maintain a high strength at elevated temperatures, also creates a challenging environment for the cutting tool [1]. Limitations in productivity when machining titanium is governed primarily by high wear rates to the cutting tool [2]. As higher cutting speeds are employed, the low thermal conductivity of the workpiece (6.7 W/m K for Ti–6Al–4V) results in temperatures exceeding 900 °C at the cutting edge which further accelerates tool wear [3]. Furthermore, the strong affinity for titanium to react with the cutting tool material is enhanced at elevated temperatures and contributes to tool wear via diffusive and adhesive mechanisms [4]. For these reasons, machining wrought Ti–6Al–4V with conventional cemented tungsten carbide (WC–Co) cutting tools is typically carried out at conservative cutting speeds; in the range of 30–60 m/min [5]. In comparison, cutting speeds exceeding 600 m/min can result in acceptable tool wear rates when machining aluminum alloys with similar tooling [6].

The limitations in productivity associated with titanium machining have motivated research and development in a number of areas with the aim to improve material removal rates (MMRs) through reducing tool wear and facilitating higher cutting speeds. These areas include: (i) cutting fluid chemistry and cutting fluid delivery methods [7,8], (ii) cryogenic coolant technologies [9,10], (iii) coatings for cemented carbide cutting tools [11,12], (iv) cutting tool geometry [13–15], and (v) the development of superhard tool materials such as polycrystalline

* Corresponding author at: Department of Materials Science and Engineering, University of Sheffield, Sir Robert Hadfield Building, Mappin Street, Sheffield, S1 3JD, UK.
E-mail address: t.m.childerhouse@sheffield.ac.uk (T. Childerhouse).

https://doi.org/10.1016/j.wear.2023.204791
Received 16 September 2022; Received in revised form 24 December 2022; Accepted 13 January 2023
Available online 24 March 2023

diamond (PCD) and polycrystalline cubic boron nitride (PCBN) [16]. The development of superhard cutting tool materials for titanium machining applications has seen significant research attention in recent years. Studies have demonstrated superior wear resistance of PCD tooling when machining titanium alloys at high cutting speeds, when compared to cemented carbide [17] and PCBN [18,19]. Other performance advantages of PCD have been highlighted by its capability to generate surfaces with excellent surface roughness characteristics [17,20]. However the development of grades for specific applications, particularly in milling processes, is still required such that the performance benefit offered by these tool materials justifies their relatively high cost. Therefore, cemented carbides remain the material of choice for machining titanium alloys, due to their high fracture toughness and hardness properties, which are retained at the typical cutting temperatures associated with conservative cutting speeds [21].

Development of cemented carbide grades for better performance in titanium alloy machining applications is possible by altering the WC grain size to adjust the hardness to toughness relationship and altering the Co binder content to modify the toughness to plastic deformation resistance properties [22]. Additionally, the wear performance of cemented carbide grades can be improved through the use of coatings which act as a protective layer on the surface of the tool. Coatings have been demonstrated to reduce adhesive wear by reducing friction and lowering the temperature at the tool/chip interface [23]. Superhard cutting tool materials, such as PCD, offer higher levels of hardness in comparison to cemented carbide which are retained at higher temperatures [3,24]. These properties mean that PCD cutting tools have the potential to perform under the extreme temperatures generated when machining at higher cutting speeds. Furthermore, the higher thermal conductivity of PCD (200–600 W/m K) compared to WC–Co (70 W/m K) can reduce the tendency for diffusion driven wear mechanisms [25,26].

Preceding research into the use of PCD cutting tools predominately focus on turning. Various wear mechanisms have been reported, such as: (i) adhesion, (ii) grain pull-out, and (iii) fracture of the cutting edge, with such mechanisms contributing to wear of the flank and/or rake faces of the tool. Lindvall et al. [27] reported diffusion driven crater wear as a dominant wear mechanism during PCD turning of Ti–6Al–4V. Temperatures exceeding 1100 °C were identified at the cutting zone when machining at a cutting speed of 300 m/min. At these conditions, diffusional loss of carbon into the workpiece was found to have occurred. Additionally, a (Ti,V)C Tool Protective Layer (TPL) was shown to have formed on the cutting edge due to the presence of the Co binder, thereby reducing the rate of diamond loss by acting as a diffusional barrier. In turning of Ti-6Al-2Sn-4Zr-6Mo, Pretorius et al. also identified crater wear as being a dominant tool degradation mechanism [25]. The grain size of the PCD was shown to have a critical effect on tool life, with a multi-modal PCD grade featuring an average diamond grain size of 14 μm being the highest performing — achieving an 80 min tool life at a cutting speed of 200 m/min. The coarsest grain size studied (39 μm) revealed that transgranular fracture of the PCD was the dominant wear mechanism. This was attributed to the lower strength associated with the large grain size material. These observations differ to those by Lindvall et al. who demonstrated that the higher Co content associated with fine grained (1 μm) PCD was able to provide a more effective diffusional barrier by forming a more continuous TPL compared to that formed during machining with a multi-modal grade. In a Ti–6Al–4V turning study by Li et al. [28], increasing diamond grain size was shown to provide a greater resistance to adhesive wear. This was attributed by the authors to be due to the higher thermal conductivity of the tool. A PCD grade featuring a multi-modal grain size distribution was also studied. In this instance, adhesion was found to be less significant and fracture to the cutting edge was shown to be the dominant wear mechanism. The significant variations observed regarding the effect of PCD material properties and dominant wear mechanism during turning of Ti–6Al–4V in these studies highlights the high sensitivity of PCD tool materials to process parameters and cutting conditions.

In milling processes, intermittent engagement of the cutting edge with the workpiece results in different thermal and mechanical conditions for the tool compared to turning. During milling, cyclic thermal and mechanical stresses on the cutting edge are more significant which increases the tendency for fracture of the cutting edge due to mechanical fatigue [29]. In face milling of Ti–6Al–4V, Li et al. [30] identified edge chipping and spalling (flaking to the rake face of the tool following the repeated removal of adhered material) to be the dominant wear mechanisms. Oosthuizen et al. reported better wear performance of PCD compared to coated WC–Co tooling in high speed (100–500 m/min) shoulder milling of Ti–6Al–4V [3]. An optimum cutting speed of 200 m/min was determined, with the authors suggesting that at such speeds, the cutting temperatures would be sufficient for an α to β phase transformation of the workpiece to occur, thereby reducing its shear strength through increasing the available number of slip systems. By increasing the cutting speed further, the tendency for adhesion driven wear also increased with a deleterious affect on tool life. The study also highlighted that at very high speeds (500 m/min) acceptable tool wear levels could be attained during PCD milling by reducing the feed rate, whilst still achieving high MRRs.

Despite the substantial research regarding the wear performance of PCD tool materials, the surface integrity of titanium alloys following surface generation with PCD tooling has received less attention. Due to higher cutting speeds which drive workpiece temperatures beyond those experienced during WC–Co machining, the affects of workpiece softening and potential for α to β phase transformation, could alter the microstructural response of the workpiece during machining. This is an area which remains to be fully explored and has the potential to have implications on the in-service performance of PCD machined titanium alloy components.

1.1. Aims and objectives

The aims and objectives of this study are as follows:

- Compare the performance and wear mechanisms of PCD and coated carbide cutting tool materials in a square shoulder milling application of titanium alloy Ti-54M employing cutting parameters appropriate for finishing.
- Investigate the influence of PCD grain size on tool life and wear behaviour.
- Investigate the effect of cutting edge microgeometry for PCD tooling, through the comparison of different cutting edge radii.
- Assess the influence of high speed PCD milling on surface integrity by characterisation of the workpiece's machining affected microstructure and surface finish.

2. Experimental method

2.1. Square shoulder milling experiment

Cutting tool trials were carried out using square shoulder milling performed with a DMG Mori DMU Evo-40 machining centre. Shoulder milling is a versatile milling process suited for the generation of perpendicular wall and floor surfaces by a combination of peripheral and face milling. A schematic representation of the process is provided in Fig. 1. The tool assembly was supplied by Seco Tools and consisted of a 25 mm diameter (d_c) Turbo-10 cutter (R217.69-2525.3-10–4A) installed in a HSK-63A Weldon side-lock holder. Respective dimensions for axial, a_p and radial, a_e cutter engagement were 0.50 and 19.0 mm and a cutter offset, $(d_c\text{-}a_e)/2$, of 3.00 mm was employed to facilitate the generation of a thick-to-thin chip geometry (i.e. climb milling).

To eliminate potential run out issues and uneven tool wear across the cutting edges, all trials were carried out employing single point

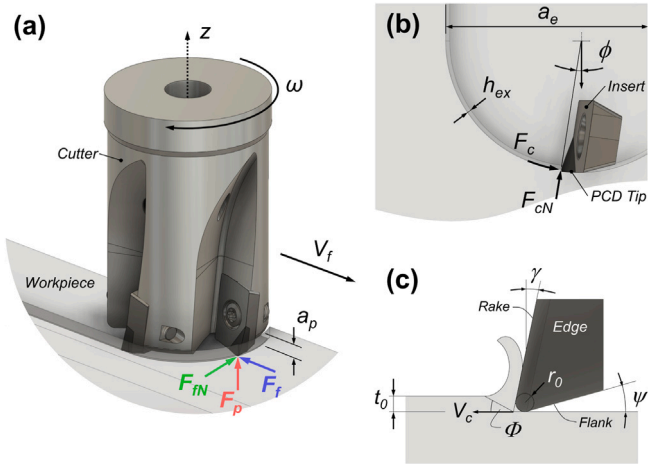

Fig. 1. Schematics illustrating the square shoulder climb milling process used for the cutting tool trials: (a) Shows the Seco Tools Turbo-10 cutter engaged in the workpiece material with annotations given for the principle cutting force directions, (b) a schematic in the plane normal to the spindle axis showing the PCD tipped insert highlighting the F_c and F_{cN} cutting force directions, and (c) the cutting edge with annotated microgeometry features.

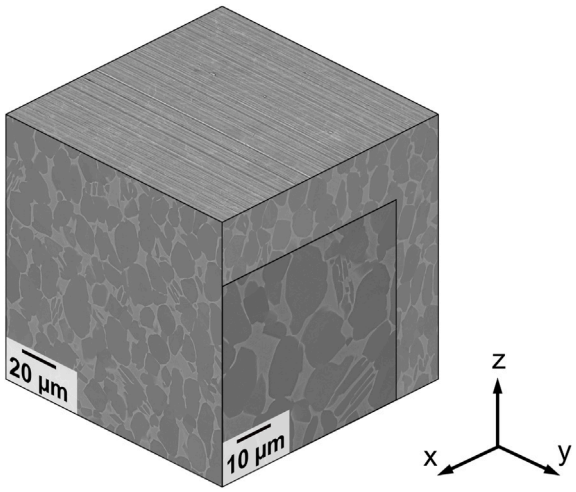

Fig. 2. Microstructure of the Ti-54M workpiece material in the as-forged, mill-annealed condition.

milling with a single insert fitted in the cutter. Throughout the trials Blaser Swisslube Vasco 7000 high pressure coolant was directed at the cutting edge via through tool delivery at a pressure of 50 Bar and concentration of 5%–8%.

For this study, the α+β titanium alloy Timetal® 54M (Ti-54M) was selected for the workpiece material. Ti-54M has been shown to display similar to slightly improved machinability characteristics to Ti–6Al–4V [31,32] and can be considered to be representative of a typical titanium alloy used in many structural aerospace component applications. The material was supplied by TIMET UK Ltd. in the as-forged, mill-annealed condition and featured the chemical composition provided in Table 1. The workpiece microstructure is shown in Fig. 2 showing a bi-modal α+β morphology consisting of equiaxed primary α grains with prior β grains containing colony α also dispersed within the structure. The residual β phase (appearing light) can be seen at the grain boundaries.

The cutting tool grades and associated cutting parameters selected for the study are shown in Table 2. Parameters are representative of typical finishing conditions. Initial benchmarking trials were conducted with cemented carbide inserts grades, F40M and MS2050

Table 1
Chemical composition of the initial Ti-54M workpiece material. All values given in wt.%.

Al	V	Mo	C	Fe	O	N	Ti
5.18	3.99	0.78	6E−4	0.45	0.16	3E−3	Bal.

(XOMX10T304TR-ME07), supplied by Seco Tools. Both inserts featured PVD (physical vapour deposition) applied coatings, which for the F40M grade comprised of a TiAlN-TiN composition and for the MS2050 grade a TiAlN-NbN composition. Trials with the carbide tooling were initially carried out at a conservative MRR and then at a higher MRR comparable to that achievable with the PCD tooling, by increasing the feed rate. Parameter screening trials were then conducted with inserts of the same geometry tipped with three different PCD grades featuring fine, PCD(A), intermediate, PCD(B), and multi-modal, PCD(C), grain sizes, as detailed in Table 3. These were supplied by Seco Tools and Element Six. For these trials, the MRR was maintained at a constant level and optimum cutting parameters, to achieve maximum tool life, were determined for each grade type by increasing the cutting speed and reducing the feed rate accordingly. To conclude, trials were carried out using the PCD(A) and PCD(B) grades following honing of the inserts to produce cutting edges featuring an edge radii, r_0 greater than that of the as-received (r_0~8 µm) geometry. Three progressively increasing hone geometries were used (small, medium, and large) with the large hone being comparable to the WC–Co edge geometry. For the edge preparation, a brush honing technique was employed producing a smooth asymmetrical 'waterfall' type edge geometry, unlike the carbide inserts which featured 'reverse waterfall' edge geometry. Edge radii and asymmetry (k-factor) values are provided in Table 2.

Aside from modifications to the edge radius, the tool edge microgeometry of the PCD tooling was not altered and featured effective rake (γ) and clearance (ψ) angles of +23° and 7° respectively when installed in the cutter. In comparison the WC–Co tooling featured γ = +28.4° and ψ = 7°. In square shoulder milling, the insert included angle is 90°, producing a maximum uncut chip thickness, t_0 equivalent to the feed rate, f_z. Finally, all tools featured a nose radius of 0.40 mm.

2.2. Characterisation techniques

For comparison of tool wear rate, measurements of the maximum flank wear land width, VB_{Max} were taken periodically using an Alicona InfiniteFocusSL 3D optical measurement system. The same system was used to assess the machined surface topography and roughness metrics. To evaluate and compare tool life, a maximum flank wear criterion of VB_{Max} of 200 µm was employed throughout the study. High resolution imaging of the machined surfaces was performed using a Hitachi TM3030 desktop scanning electron microscope. Further characterisation of cutting tool wear morphology, as well as microstructural analysis of the workpiece material, was performed using an FEI Inspect F50 field emission gun scanning electron microscope using secondary electron (SE) and back-scattered electron (BSE) imaging. It is notable that no etching or chemical cleaning was performed on the cutting edges prior to SE/BSE imaging.

2.3. Cutting force analysis

Cutting force data was captured with the inclusion of a Kistler type 9139AA dynamometer plate in the workholding setup which is shown in Fig. 3. Force signals were acquired in the feed, F_f, normal, F_{fN}, and axial, F_p directions, as shown by Fig. 1a. Transformation of the acquired cutting forces from the measured workpiece co-ordinate system to the co-ordinate system fixed to the rotating cutting edge is given by Eq. (1) [33], where ϕ is the instantaneous angular position

Table 2
Cutting parameters and cutting edge radii in the 'as-received' and 'honed' condition used during the single point milling trials. Specific values for r_0 in the 'honed' condition have not been provided at the request of the tooling manufacturer.

Grade Type	Cutting Speed	Feed Rate	MRR	Cutting Edge Radius, r_0		Edge Asymmetry
	V_c [m/min]	f_z [mm/tooth]	[cm^3/min]	As-rec. [μm]	Honed	K-factor
F40M	60	0.08, 0.10	0.58, 0.73	34.1 ± 3.0	–	1.52 ± 0.07
MS2050	60	0.08, 0.10	0.58, 0.73	55.3 ± 0.9	–	1.28 ± 0.19
PCD(A)	200–600	0.030–0.010	0.73	8.8 ± 0.5	Small, Med, Large	0.67 ± 0.03[a]
PCD(B)	200–600	0.030–0.010	0.73	9.6 ± 1.9	Small, Med, Large	0.64 ± 0.02[a]
PCD(C)	300–600	0.020–0.010	0.73	8.3 ± 2.3	–	1.11 ± 0.17

[a]The K-factor values for PCD(A) and PCD(B) correspond to the honed condition. Typical K-factors for the as-received condition were comparable to the PCD(C) grade.

Table 3
PCD insert grades and corresponding thermal and mechanical properties. At the request of the manufacturer, PCD grain size along with thermal conductivity, transverse rupture strength, and fracture toughness properties have been normalised with respect to the highest value displayed across the various grades.

Grade type	Avg. grain Size	Grain distribution	Thermal conductivity			Transverse rupture strength	Fracture toughness
			20 °C	500 °C	1000 °C		
PCD(A)	0.03	Unimodal	0.36	0.56	0.14	1.00	1.00
PCD(B)	0.33	Unimodal	1.00	0.80	0.24	0.79	0.67
PCD(C)	0.07–1.00	Multi-modal	0.93	0.88	0.26	0.65	0.70

of the cutting edge (Fig. 1b). This yields the force components in the cutting, F_c and tangential directions, F_{cN}:

$$\begin{bmatrix} F_c \\ F_{cN} \end{bmatrix} = \begin{bmatrix} -sin(\phi) & cos(\phi) \\ cos(\phi) & sin(\phi) \end{bmatrix} \begin{bmatrix} F_f \\ F_{fN} \end{bmatrix} \quad (1)$$

here, the angular position of the cutting edge upon engagement with the workpiece, ϕ_{en} is given by:

$$\phi_{en} = 90° - cos^{-1}\left[(R - a_e)/R\right] \quad (2)$$

where R is the cutter radius. Upon exit of the cutting edge with the workpiece, $\phi_{ex} = 90°$, corresponding to a chip thickness, $t_0 = 0$.

3. Results and discussion

3.1. Wear performance of the PCD and carbide grades

Flank wear as a function of total cutting time when machining with the carbide tooling is plotted in Fig. 4. The two grades show similar performance for the two coatings when machining at the more conservative parameter set, with $VB_{Max} < 125$ μm after 50 min of cutting (corresponding to a material removal vol. of 29 cm^3). When increasing the feed rate, the wear rates for both grades increased significantly. Better performance was displayed by the MS2050 in comparison to the F40M grade, with respective tool lives of 32 min (23.4 cm^3) and 27 min (19.7 cm^3) attained when applying a flank wear criteria of $VB_{Max} = 200$ μm.

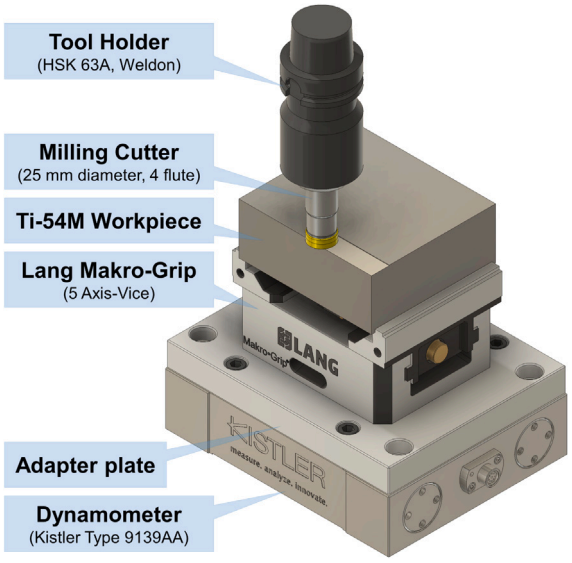

Fig. 3. Schematic illustrating the machining and workpiece setup with cutting force data acquisition hardware.

The flank wear evolution attained during machining with the PCD(A) grade is shown in Fig. 5a. Increasing the cutting speed and simultaneously reducing the feed rate is shown to have a beneficial effect on tool life until parameters of $V_c = 450$ m/min and $f_z = 0.0134$ mm/z are reached. Beyond this, continuing to increase the cutting speed and reduce the feed rate is shown to have a detrimental effect on tool life. The flank wear rates for the PCD(B) and PCD(C) grades are shown in Figs. 5b and c, respectively. The tool life attainable during machining with each of these grades is considerably shorter than that of the PCD(A). Optimum cutting parameters to achieve the longest tool life for these grades were found to be 500 m/min, 0.012 mm/z. However it is notable that for the PCD(C) grade in particular, marginal improvements in tool life were attainable through altering cutting parameters.

The evolution in morphology of the wear observed on the carbide tooling is shown in Fig. 6. The wear scars experienced by both grades are located predominantly at the nose of the tool, corresponding with the region of the cutting edge which engages the uncut chip. No wear features were visible further along the cutting edge. During the early stages of tool life, a more significant loss of tool material can be seen to occur when machining with the MS2050 grade. As cutting time increases, the loss of tool material in both cases increases at a gradual rate and is dominated by wear directly to the cutting edge, contributing to an increase in VB_{Max}. For both grades, the wear morphologies observed suggests mechanically driven wear mechanisms are responsible for tool degradation. As the total cutting duration increases beyond 26 min, differences in the performance of the two grades becomes apparent, with the MS2050 grade continuing to wear gradually, whereas the F40M grade experiences severe chipping.

The wear morphology progression for the PCD(A) grade when machining at the optimum parameter set is shown in Fig. 7a. During the early stages of machining, the loss of tool material is negligible. Wear features include notching (Fig. 7a-i) and adhesion, leading to the formation of an adhered layer of material at the cutting edge (Fig. 7a-ii). As the cutting duration increases, the loss of a layer of material from the rake face, near to the nose of the tool, can be seen to have occurred

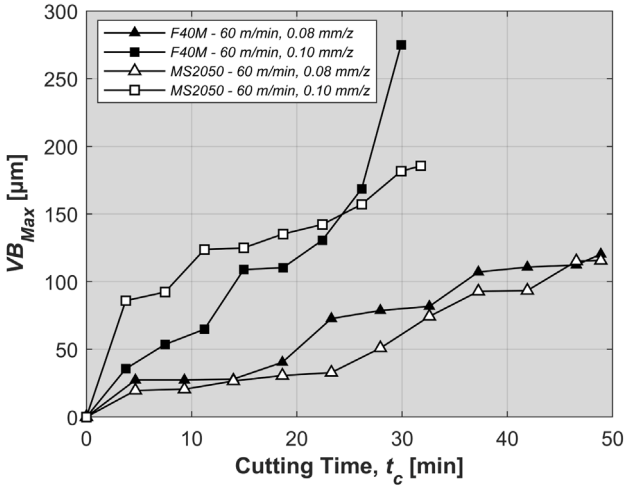

Fig. 4. Flank wear progression with increasing cutting time comparing the coated carbide grades.

(Fig. 7a-iii). Similar wear features, involving flaking of material from the rake face have been observed during PCD turning [27,28,34] and milling of Ti–6Al–4V [30]. However, in the case of milling, this has only been at cutting speeds exceeding 250 m/min. The generation of this feature can be attributed to a mechanism referred to as 'spalling', whereby tool material is lost through a cyclic process of workpiece adhesion followed by the removal of the adhered layer along with the pull-out of welded PCD grains.

The wear morphology experienced by the PCD(B) and PCD(C) grades when machining at 500 m/min, 0.012 mm/z are shown respectively in Figs. 7b and c. Loss of tool material due to mechanical fracture at the cutting edge is shown to be the predominant wear mechanism. Unlike the coarser grained PCD grades, the fine grained PCD(A) material is able to provide the longest tool life due to its ability to resist degradation mechanisms dominated by mechanical fracture and operate under conditions where the thermal load is more pronounced. This was not observed for the PCD(B) and PCD(C) materials, whereby mechanical failure was shown to be the predominant tool degradation mechanism throughout the parameter range investigated.

The superior performance of the PCD(A) grade compared to the coarser grained PCD can be attributed to the greater fracture toughness and rupture strength properties displayed by the fine grain size. Such properties are critical during the intermittent cutting processes, to resist fracture initiation due to cyclic mechanical stresses subjected to the cutting edge. The higher levels of thermal conductivity possessed by the coarser grades, which, in some instances, have proven to provide better resistance to chemical and diffusional wear during turning [25], can be seen to be of secondary importance during milling due to the higher rates of wear when the tool is subject to mechanical fracture compared to spalling.

For the PCD(A) material, a transition from mechanical fracture to a spalling dominated wear mechanism was observed as cutting speed was increased and the feed rate was simultaneously reduced. Fig. 8 shows how the wear morphology changes as cutting speed is increased from 400 to 500 m/min, highlighting an increase in adhered material and spalling as cutting speeds are increased beyond 450 m/min. When machining at higher cutting speeds, spalling was shown to have initiated at an earlier point in the overall life of the tool. Specifically, when machining at speeds of 500 and 600 m/min this feature initiated after 7.5 and 1.9 min, respectively.

The tendency for increased spalling as the cutting parameters shift from low speed/high feed to high speed/low feed milling can be attributed to a combination of possible factors. The reduction in feed rate will result in a smaller contact area between the cutting edge and uncut

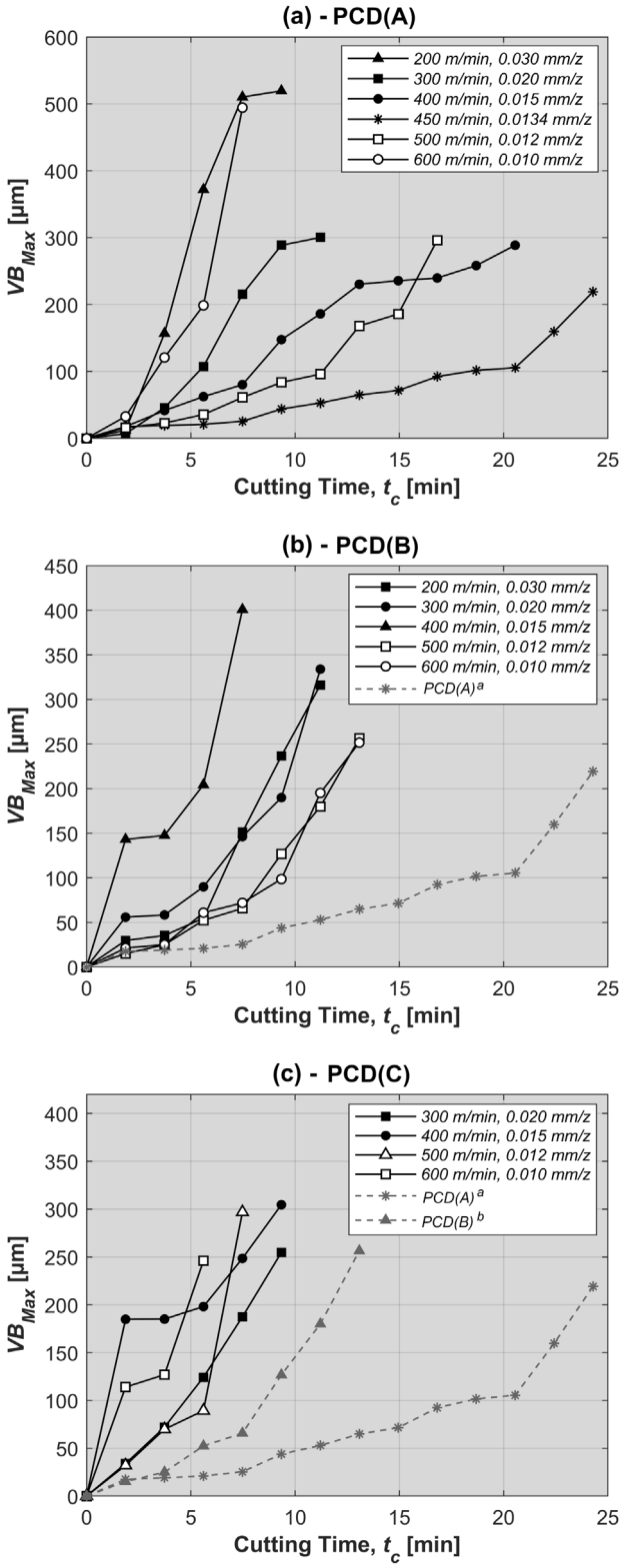

Fig. 5. Flank wear progression with increasing cutting time for the: (a) PCD(A), (b) PCD(B), and (c) PCD(C) tool grades. ([a]PCD(A) comparison at 450 m/min, 0.0134 mm/z and [b]PCD(B) comparison at 500 m/min, 0.012 mm/z).

chip. This will result in an increase in the concentration of contact stresses applied at the cutting edge, this location is shown in Fig. 8ii and iii to be where adhered material is most concentrated. This increase in local pressure between the tool and uncut chip will promote adhesion of

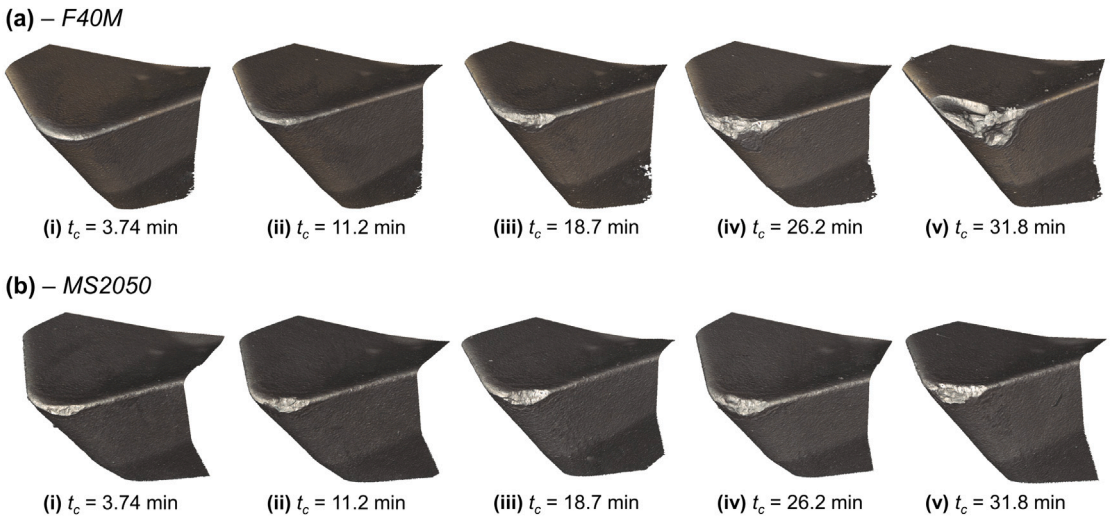

Fig. 6. Wear morphology for the: (a) F40M and (b) MS2050 grades when machining at 60 m/min, 0.10 mm/z.

the workpiece material. Additionally, flaking of tool material identified further up the rake face from the cutting edge is expected to have been promoted by an increase in cyclic thermal/mechanical loads resulting from higher cutting speeds. This effect was demonstrated by Li et al. [30] to result in a similar rake wear tendency. It is expected that wear to the cutting edge in the adhesion dominated region may have also contributed to flaking at the rake face due to a degradation of the local structural integrity of the insert.

Fig. 9 provides a comparison showing the wear performance for each of the tool grades included in the study at cutting parameters which achieved their longest tool life. It is notable that the comparison of tool life focuses on the flank wear metric and does not account for material loss at the rake face. During the early stages of overall tool life, the greatest resistance to flank wear was achieved by the PCD(A) and F40M grades, which were shown to have the lowest wear levels measured up to a total cutting time of 21 min. However, as the total cutting time increases towards the end of tool life, the MS2050 grade was shown to offer the longest tool life (32 min, 23.4 cm^3) compared to the PCD(A) (24 min, 17.5 cm^3). The rapid increase in wear rate for the PCD(A) tool occurring following t_c = 21 min can be attributed to the onset of mechanical fracture resulting from fatigue stresses concentrated at the cutting edge. During the spalling wear cycle, tool material is lost from the rake face contributing to a deterioration of the cutting edge and a rise in cutting forces, making the tool more susceptible to mechanical failure.

3.2. Cutting force response

For the following analysis, the measured cutting forces have been transformed from the workpiece co-ordinate system to the co-ordinate system fixed to the rotating cutting edge by the transformations given by Eq. (1). This yields the force components subjected to the cutting edge in the cutting, F_c and tangential directions F_{cN}. An example of the cutting force response versus instantaneous cutter position ϕ, when machining with the MS2050 tool is shown in Fig. 10. The cutter engagement period is highlighted and is clearly visible from the sharp force transient which corresponds with cutting edge engagement, ϕ_{en} = −31.3°. Following this peak, a fall in cutting force can be observed, particularly in the F_c and F_{cN} directions as the cutting edge sweeps through the uncut material. This can be attributed to the reduction in the uncut chip thickness during the engagement period. At the point where the cutting edge exits the material, ϕ_{ex} = 90°, forces fall to near zero. During the rotational period where the cutting edge is disengaged with the workpiece, the F_c force component remains near zero, whereas

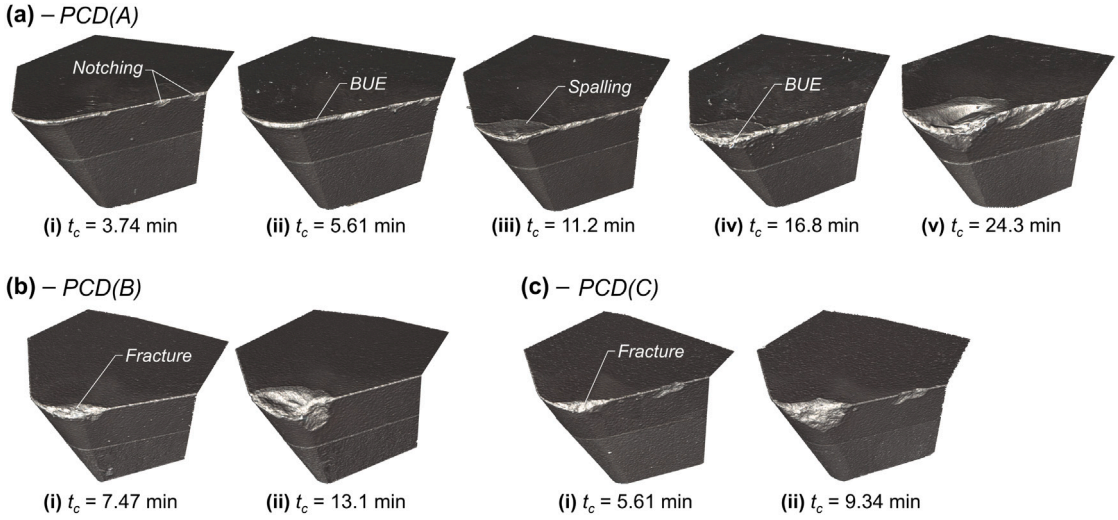

Fig. 7. Wear morphology for the: (a) PCD(A) grade when machining at 450 m/min, 0.0134 mm/z, and the (b) PCD(B) and (c) PCD(C) grades when machining at 500 m/min, 0.012 mm/z.

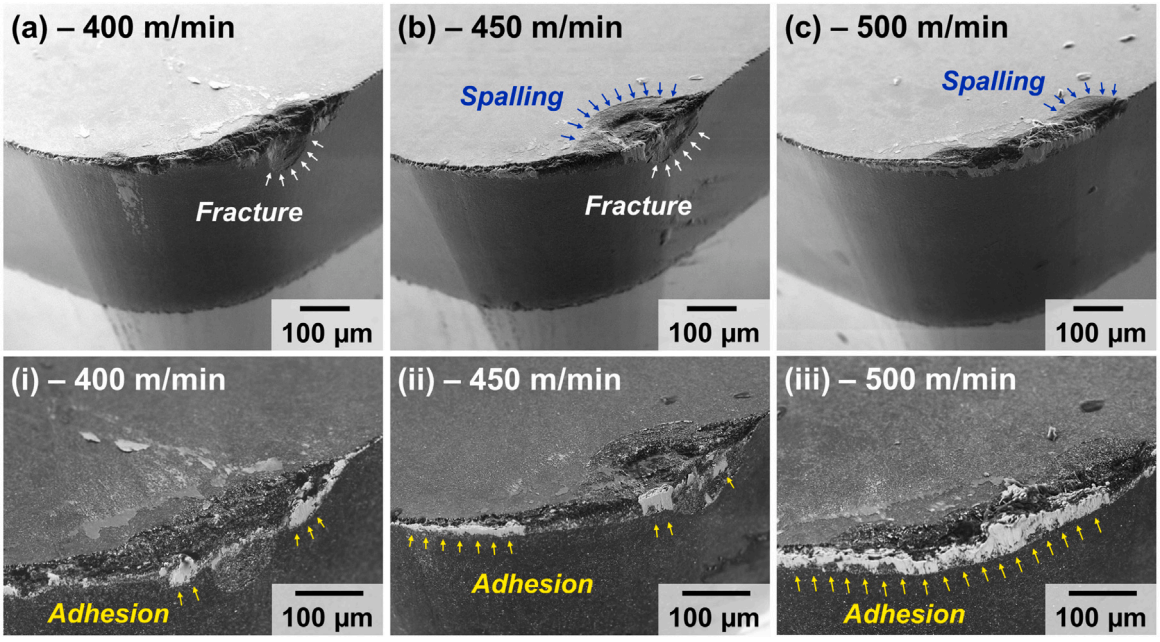

Fig. 8. Wear scar morphology of the PCD(A) tooling showing the transition from fracture to spalling dominated wear as the cutting speed is increased. (a) Shows an SE image of the cutting edge when machining at 400 m/min, 0.015 mm/z following t_0 = 11.2 min, (b) - 450 m/min, 0.0134 mm/z following t_0 = 11.2 min, and (c) - 500 m/min, 0.012 mm/z following t_0 = 7.47 min. BSE images of the cutting edges in (a) - (c) are provided in (i) - (iii) showing the presence of Ti-54M workpiece material (light) adhered to the PCD cutting edge (dark).

in the F_{cN} and F_p directions a low level of cutting force is maintained due to rubbing contact between the newly machined surfaces and the cutting edge. The small gradual increase observed in F_{cN} during the out-of-cut period is expected to be a result of the cutting edge rubbing over material machined during the previous pass of the tool.

A comparison between the cutting force response versus total cutting time for the MS2050 and PCD(A) tool materials, when machining at parameters which allow for their respective optimum tool lives, is shown in Fig. 11. The data plotted corresponds to the peak cutting forces observed at ϕ_{en}. Comparing the two tools shows considerably higher forces when machining with the WC–Co insert and this trend can be seen for all three force component directions. The main factor contributing to this difference in force response can be attributed to the contrast in cutting parameters employed when machining with the two tools. Due to the difference in wear characteristics, optimum parameters for machining of titanium alloys with WC–Co tooling employ significantly higher feed rates and lower cutting speeds than those achievable with PCD tool materials. The greater uncut chip thicknesses associated with this higher feed rate machining will contribute to greater cutting forces, particularly in the F_c direction.

The cutting force contribution associated with workpiece ploughing is also expected to have had a role on the differences in cutting forces. Ploughing is promoted when the ratio between the cutting edge radii and un-cut chip thickness is higher, as under such circumstances a greater portion of the un-cut chip is locally subjected to a negative rake angle and has a higher tendency to pass beneath the cutting edge rather than forming the chip [35]. The MS2050 inserts featured an edge radii, r_0 = 55 µm. When machining at f_z = 100 µm/z, the

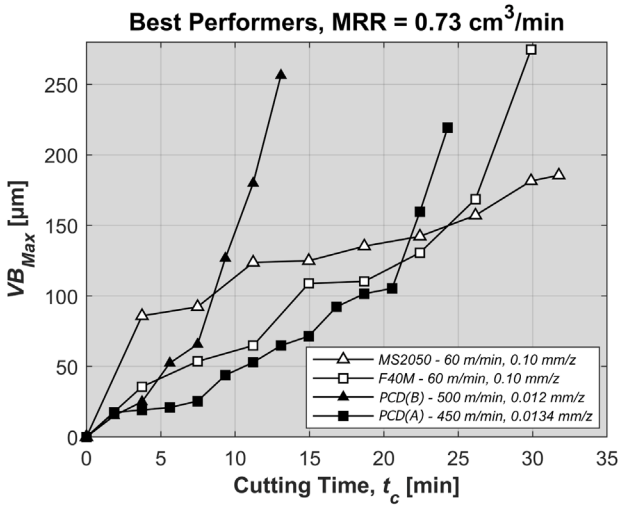

Fig. 9. Flank wear progression with increasing cutting time comparing PCD and coated carbide grades at the parameters which achieved the longest tool life at a MRR = 0.73 cm^3/min.

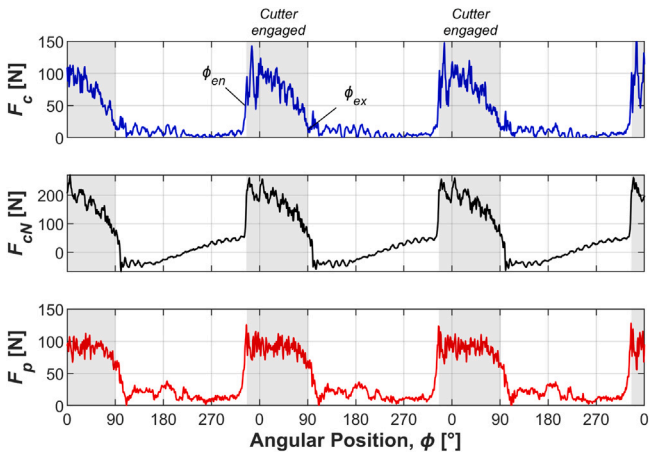

Fig. 10. Cutting force response for the MS2050 tool in the 'as-received' condition when machining at 60 m/min, 0.10 mm/z. Forces have been transformed into the co-ordinate system fixed to the rotating cutting edge.

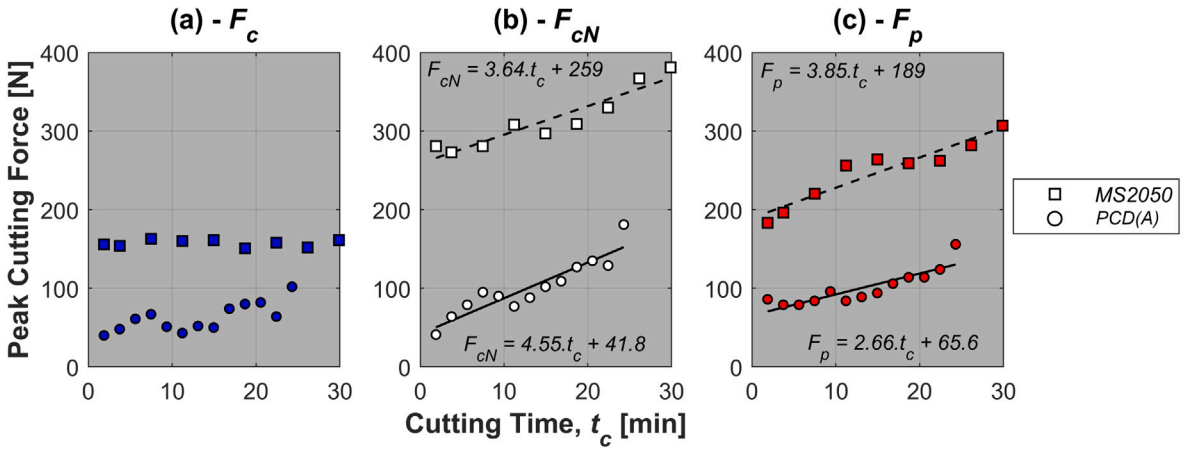

Fig. 11. Cutting force response with increasing cutting time comparing the performance of the MS2050 (60 m/min, 0.10 mm/z) and PCD(A) (450 m/min, 0.0134 mm/z) grades. MRR = 0.73 cm^3/min in both cases.

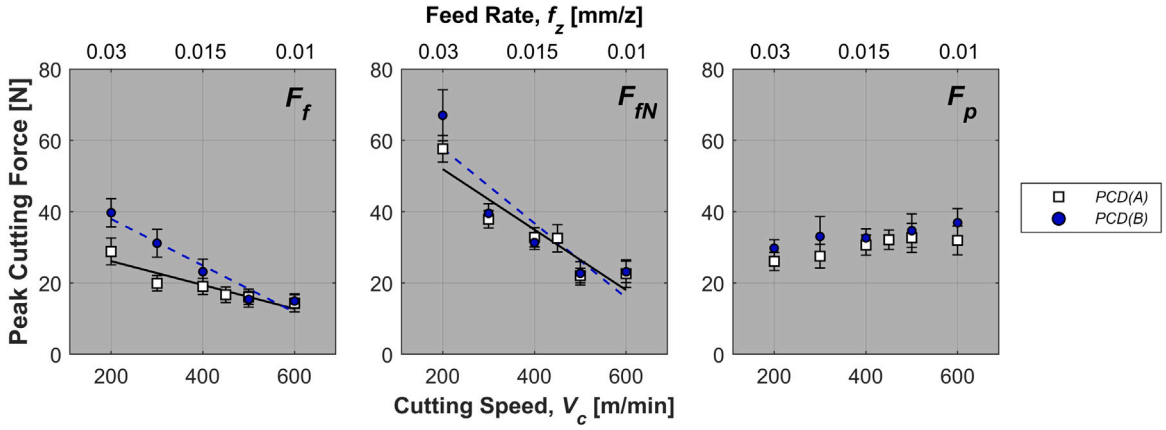

Fig. 12. Cutting force response showing the influence of cutting parameter selection comparing the performance of the PCD(A) and PCD(B) grades with edge geometries in their 'as-received' condition.

ratio for r_0/f_z = 0.55. For the PCD(A) tooling the edge radii was significantly sharper, r_0 = 8 μm. However, the feed rates employed were considerably lower, f_z = 13.4 μm/z, resulting in a ratio for r_0/f_z = 0.60. These values would suggest that the ratio of ploughing induced cutting forces is roughly similar when machining with either the PCD(A) or MS2050 tooling. As the cutting forces associated with chip formation, F_c are considerably higher when machining with the WC–Co tooling, the overall force magnitude associated with ploughing will be greater than those induced during machining with the PCD tools. This effect can be observed in Fig. 11, which indicates a significant increase in forces in the ploughing dominated F_{cN} and F_p directions versus the F_c direction when machining with the MS2050. In comparison, the cutting force response for the PCD(A) tooling shows similar forces in each of the F_{cN}, F_p and F_c directions.

The influence of cutting parameter selection on the force response during machining with the PCD(A) grade in the non-honed condition is shown in Fig. 12. To ensure that the affects of any edge geometry alteration resulting from tool wear did not influence the results, data was taken when using a new cutting edge from the average peak cutting forces during the first 10 rotations of the tool following initial cutter engagement (i.e. at $t_c \rightarrow 0$). The error bars shown represent ±1 standard deviation from these data. A strong correlation is apparent showing a decrease in cutting forces in the feed, F_f and normal, F_{fN} directions as the cutting parameters transition from low speed/high feed to high speed/low feed conditions. The axial cutting forces, F_p however remain more consistent through the transition in cutting parameters. This reduction in cutting force response can be primarily attributed to a reduction in the uncut chip thickness and a reduced chip load on the cutting edge. It is notable that this reduction in cutting forces corresponds with an improved wear performance in the mechanical fracture dominated wear region as cutting speed increases from 200 to 400 m/min. This suggests that a reduction in the cyclic fatigue stresses subjected to the cutting edge has had a favourable effect on tool life, when operating in the fracture dominated wear region. To further enhance tool life, changes to the cutting strategy from climb milling, as used in the present study, to an up milling (thin-to-thick chip generation) approach may be considered. This may be beneficial at reducing both fracture and adhesion/spalling tendencies of PCD tooling by reducing the cyclic impact loading, which acts on the cutting edge in the F_f and F_{fN} directions.

When machining at low cutting speeds/higher feed rates, fracture of the cutting edge was revealed to be the predominant wear mechanism for the PCD grades. In addition to the aforementioned effects of feed rate and higher chip load contributing to mechanical failure of the tool, the tendency for fracture to occur when machining at these parameters could also be partially attributed to lower workpiece temperatures associated with the slower cutting speeds. Increasing the workpiece temperature during machining of alloys such as Ti–6Al–4V, through workpiece pre-heating [36] and laser assisted machining [37], have been demonstrated to offer benefits to tool life due to thermal softening of the workpiece and a reduction in cutting forces. Similar benefits arising from thermal softening of the workpiece, resulting from increasing the cutting speed, could also provide improvements in PCD tool life in the present study. Based on the abrupt reduction in mechanical

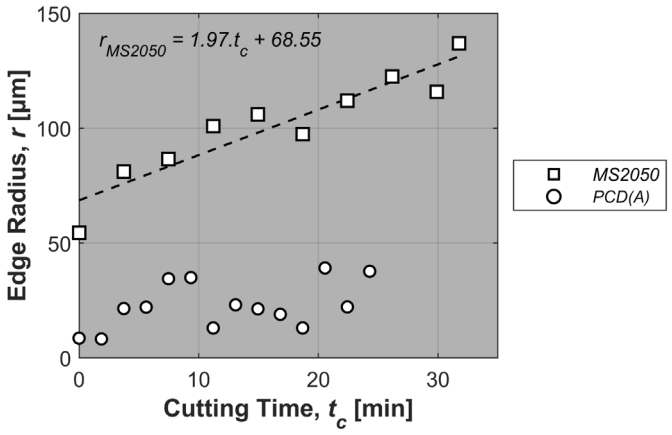

Fig. 13. Change in cutting edge radius with increasing cutting time during machining with the MS2050 (60 m/min, 0.10 mm/z) and PCD(A) (450 m/min, 0.0134 mm/z) grades.

fracture experienced by the cutting edge and the onset of spalling as cutting speeds increased from 400 to 450 m/min, thermal softening alone may not be fully responsible for the transition in predominant wear mechanism. Should temperatures within the primary shear zone have reached the β transitional temperature (~950 °C for Ti-54M) the strength of the workpiece would have reduced at a higher rate than during thermal softening in the α+β phase region. This is due to the increase in the available slip systems in the β phase [38].

Fig. 13 shows the change in cutting edge geometry for the two cutting tool materials with increasing cutting time. A strong positive correlation between the cutting edge radii and t_c is shown for the MS2050 insert as chipping to the cutting edge contributes to a degradation in the cutting edge geometry. For the PCD(A) tool, a general positive trend is also observed, however, more fluctuation in the cutting edge radii measurement is evident. This can be attributed to the spalling wear mechanism, whereby tool material is lost mainly from the rake face rather than directly at the cutting edge. Based on these changes in cutting edge microgeometry, the positive trends observed between cutting force and cutting time shown in Fig. 11, can be explained due to the increase in the ploughing effect as the cutting edge radii increases. This is particularly evident when comparing the trends for the different force components. Whereas a strong trend is evident in the F_{cN} and F_p directions, the F_c component remains mostly unaffected by the deterioration in edge geometry, as the influence of ploughing on F_c is less significant than in the normal and axial directions.

3.3. PCD wear mechanisms

Fig. 14 shows the wear morphology of the PCD(A) insert grade during the early stages of overall tool life (t_c = 3.74 min) when machining at 450 m/min, 0.0134 mm/z. In Fig. 14a, particles of adhered material, on a scale of ~10–50 µm, are clearly distinguishable along the cutting edge where the rake and flank faces meet. The adhered material is located predominantly along the region of the cutting edge which contacts the wall and floor of the workpiece material. Fig. 14b shows a high resolution image of the same cutting edge highlighting a location where adhered material has been plucked from the tool to leave a rough dimpled wear surface on the rake face of the tool. The dimples visible in this worn region shows a cylindrical type dimple morphology, which are on a similar scale to the PCD(A) diamond grain particles ~1 µm. This suggests that the removal of adhered particles has resulted in pull-out of diamond grains from the Co binder matrix by delamination, or flaking, of tool material from the rake face resulting in spalling.

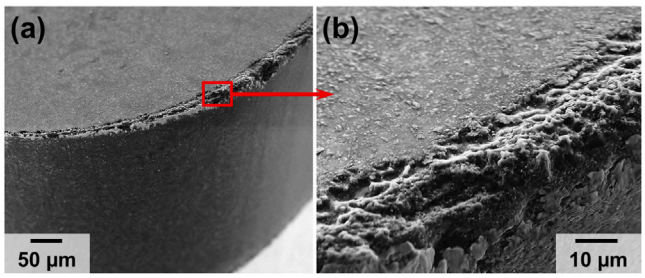

Fig. 14. Images of the PCD(A) cutting edge when machining at 450 m/min, 0.0134 mm/z following t_c = 3.74 min. (a) Shows a low resolution BSE image highlighting the presence of adhered material (light) along the PCD cutting edge (dark). (b) Shows a higher resolution SE image at a location where adhered material has been removed from the tool highlighting pull-out of PCD grains from the rake face.

Fig. 15 shows the wear morphology of the PCD(A) insert grade during the intermediate stages of overall tool life (t_c = 11.2 min) when machining at 450 m/min, 0.0134 mm/z. At this stage in the life of the tool, flaking of material from the rake face of the tool can be observed, which can be attributed to spalling. Flank wear is also observable with material loss occurring at a location directly adjacent to the wear scar on the rake face of the tool. It is assumed that the loss of material at the rake face occurring during the initial stages of the life of the tool (as shown in Fig. 14b) has resulted in a localised region of higher cutting stresses, causing fracture of material from the flank face. High resolution imaging of the rake face, shown in Fig. 15b and c, reveals a shelf-like feature, which has formed directly at the periphery of the rake face. It is expected that the formation of this feature is a result of the continuation of the spalling mechanism concentrated at the region of the cutting edge that engages the uncut chip. Unlike the crater wear morphology reported by Lindvall et al. [27] during turning of Ti–6Al–4V, the wear scar is more localised and the surface of the wear region displays evidence of severe diamond grain pull-out, rather than the smooth crater surface reported during the turning application. The dominance of spalling, rather than diffusion driven wear predominant during turning, is expected to be an effect of intermittent cutting edge engagement during milling, which provides less opportunity for diffusion. This is due to the absence of continuous sliding contact between the chip and rake face, as well as an effect of highly periodic cutting conditions (such as temperature and force) which encourage the removal of adhered workpiece material. Further work should be focused on investigating the contribution of diffusion driven wear in the present milling application and its significance as the tool is predominantly exposed to spalling induced grain pull-out.

Fig. 16 shows the wear morphologies of the PCD(B) and PCD(C) tool materials when machining at 500 m/min, 0.012 mm/z. Loss of the PCD tool material can be predominantly attributed to mechanical fracture located at the flank face of the tool. The level of fracture can be seen to be more severe for the PCD(B) grade, however at this early stage of tool life it is difficult to conclude that this grade is more susceptible to fracture due to variability in the material properties for different cutting edges. Similar to the PCD(A) grade, adhered material can also be identified along the cutting edge, however, this has not contributed to diamond grain pull-out or the formation of the spalling related wear feature identified on the rake face of the PCD(A) tooling. It is expected that this is due to the lower fracture toughness possessed by the coarser grained PCD(B) and PCD(C) grades. This reduced resistance to fracture has meant that large multi-grained particles of tool material have been able to break away from the tool, along with any adhered material, prior to the occurrence of the adhesive/abrasive spalling wear mechanism.

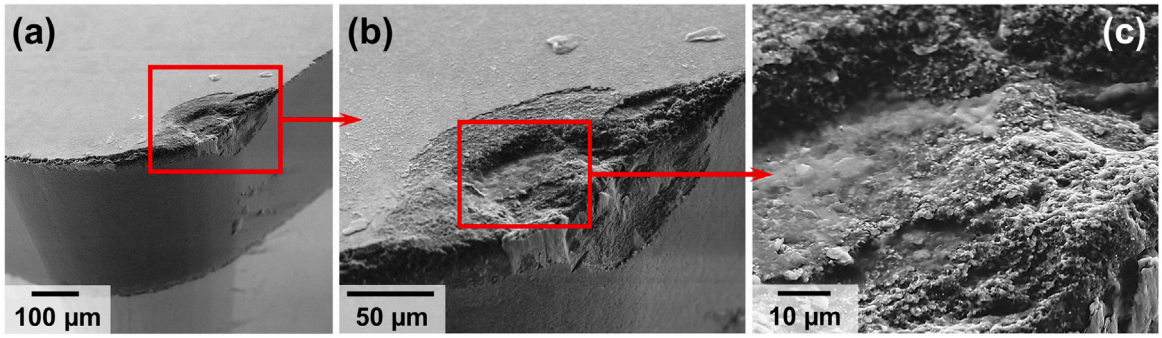

Fig. 15. SE images of the PCD(A) cutting edge when machining at 450 m/min, 0.0134 mm/z following, t_c = 11.2 min. (a) Shows a low resolution image of the cutting edge highlighting the location where spalling has occurred, (b) and (c) show higher resolution images of the spalling induced wear feature.

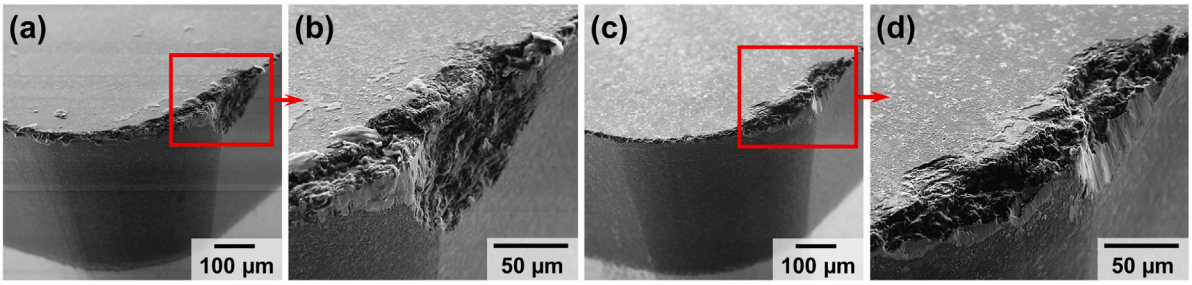

Fig. 16. SE images of the (a)–(b) PCD(B) and (c)–(d) PCD(C) cutting edges when machining at 500 m/min, 0.012 mm/z following t_c = 3.74 min.

3.4. Performance of the honed PCD grades

The wear rates for the honed PCD(A) and PCD(B) grades are shown in Fig. 17. The results presented show the tool performance when machining at the parameter sets found to offer the longest tool life for the non-honed tools. For both grades, higher rates of wear were measured when the edge radii was increased from the 'as-received' geometry. Observations for the results for the honed PCD(A) grade (Fig. 17a) show a sharp increase in VB_{Max}, corresponding with the onset of mechanical fracture to the cutting edge. As the edge hone radii is increased, fracture of the cutting edge can be seen to occur at an earlier stage in the life of the tool (at t_c = 10 min for r_0 = small, and at t_c = 5 min for r_0 = med.).

The increased tendency for mechanical fracture of the cutting edge can be attributed to an increase in cutting forces. Specifically, as the cutting edge radius is increased, the ratio between cutting edge radii and the uncut chip thickness increases significantly. This results in an increase in the area of the uncut chip subjected to a negative rake angle which promotes ploughing of the workpiece material and therefore an increase in F_{cN} and F_p forces. As highlighted in the earlier discussion, PCD tools have shown to be highly susceptible to mechanical damage, which has been promoted by the increase in cutting forces acting normal to the cutting edge profile. These findings suggest that in this application, any potential advantages of reinforcing the cutting edge through honing are outweighed by an increase in mechanical loads and causing cutting edge fracture.

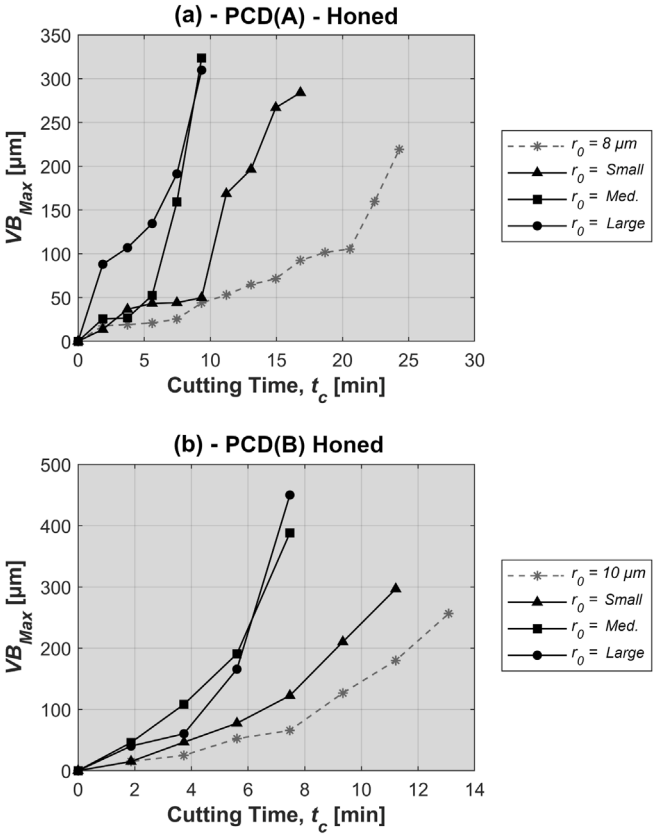

Fig. 17. Flank wear progression with increasing cutting time showing the influence of edge hone radius for: (a) PCD(A) grade at 450 m/min, 0.0134 mm/z, and (b) PCD(B) grade at 500 m/min, 0.012 mm/z.

3.5. Workpiece material response

The microstructural response of the Ti-54M workpiece material following machining with the PCD and WC–Co tooling is shown in Fig. 18. The micrographs provided show the workpiece microstructure in the plane normal to the cutter feed direction, V_f and have been annotated to show the cutting direction, V_c. The response of the workpiece material following machining with the PCD(A) tool grade as cutting speed is increased from 200 to 600 m/min and the corresponding feed rate is reduced from 0.03 to 0.01 mm/z is shown in Fig. 18a–c, and highlights

a reduction in severe plastic deformation (SPD) as cutting parameters transition to higher cutting speeds. SPD can be distinguished by sweeping of grains in the cutting direction as they approach the machined surface. Such deformation has shown to be typical of $\alpha+\beta$ titanium alloys such as Ti–6Al–4V [2,39] and Ti-54M [40] following machining. The micrographs provided have been annotated to highlight the depth of the SPD layer thickness and show deformation penetrating to a depth of 4 μm when machining at 200 m/min which reduces to 2 μm as the cutting speed is increased to 450 m/min. At 600 m/min any near surface deformation of the microstructure becomes difficult to distinguish from the bulk. It is notable that an increase in SPD layer thickness also corresponds to a greater degree of shear strain in the cutting direction which is highlighted by the 200 m/min condition.

The microstructural response following machining with the MS2050 WC–Co tooling at more conventional cutting parameters (60 m/min, 0.1 mm/z) is shown in Fig. 18d. In this instance the microstructure displays a SPD layer penetrating to 4 μm, similar to that of the PCD machined material at 200 m/min. However, unlike the PCD machined material, the level of compressive strain which can be observed in the material machined with the WC–Co tooling is much more significant. The α_p grains, which displayed an equiaxed morphology in their unaffected state, can be seen to be severely deformed as they approach the machined surface, suggesting that higher levels of compressive strain in comparison to the PCD machined material.

To understand the effect of cutting tool material and parameter selection on the workpiece's metallurgical response it is necessary to consider their influence on the thermal and mechanical conditions the workpiece surface is subjected to. The analysis discussed in Section 3.2 highlighted that the cutting forces associated with PCD machining were considerably lower compared to those during machining with WC–Co tooling, this was due to the sharper cutting edge as well as the high speed/low feed rate cutting strategy. These lower cutting forces were attributed to a reduction in the ploughed layer thickness and ploughing associated cutting forces, both of which have been shown to be linked to shear and compressive imparted strain on subsurface workpiece material [35]. This explains the findings from the metallurgical characterisation, which showed more severe microstructural deformation following WC–Co in comparison to PCD machining. The reduction in SPD layer thickness observed during machining with the PCD(A) tooling as cutting parameters transition from the low speed/high feed rate to the high speed/low feed rate strategy could also be explained by the reduction in the magnitude of cutting forces associated with ploughing as well as a reduction in the ploughed layer thickness at lower feed rates. However, as shown in Fig. 12 the change in the F_p force component is negligible over the transition in cutting parameters. This suggests that another factor may also be responsible for the material response observed. Brown et al. [35] demonstrated that during orthogonal milling, strain rate hardening had a dominant effect over cutting speed driven thermal softening of the workpiece material as cutting speeds were increased from 20 to 80 m/min. It is possible that at the extremely high strain rates associated with the cutting speeds employed in the current work that a strain rate hardening effect has increased the workpiece's resistance to plastic deformation. If this is the case, it would suggest that workpiece thermal softening may not be as significant as expected due to the competing strain rate hardening mechanism. Therefore, the observations made regarding cutting forces in Section 3.2 may be predominantly attributed to the effects of feed rate and chip load rather than softening mechanisms.

The observations of a reduction in SPD at higher cutting speeds for the PCD(A) tool (Fig. 12a–c) can be attributed to a combination of a reduction in chip load at the low feed rates employed when machining at higher cutting speeds and the aforementioned effects of strain rate hardening, increasing the workpiece's resistance to deformation. Further work involving similar trials performed at a single feed rate would be beneficial in assessing the contribution of cutting speed driven thermal softening and strain rate hardening effects on the machining response of the workpiece.

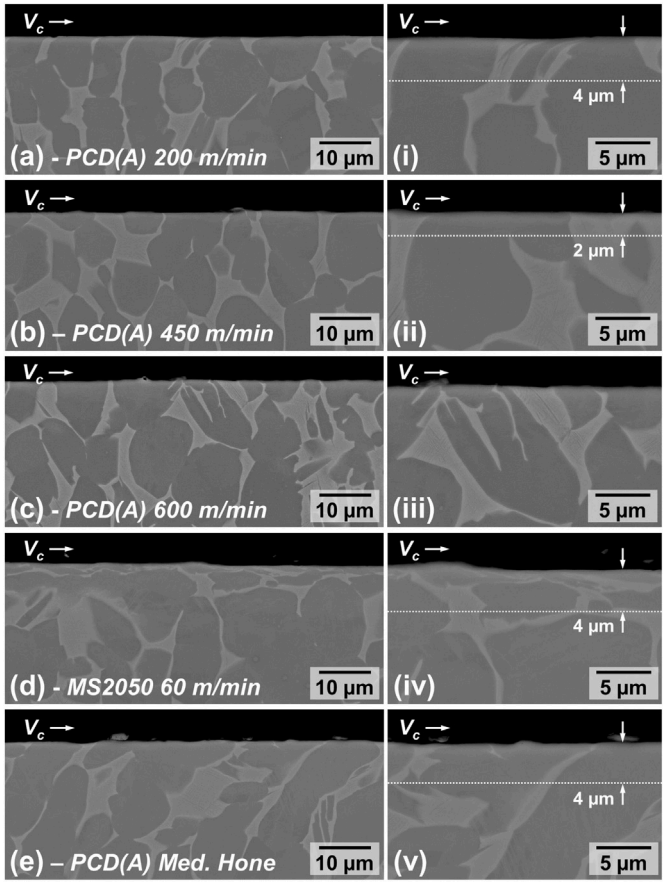

Fig. 18. BSE images showing the severity microstructural deformation induced during machining in the plane normal to the feed direction after machining with the following tooling: (a) PCD(A) 'as-received' (200 m/min, 0.03 mm/z), (b) PCD(A) 'as-received' (450 m/min, 0.0134 mm/z), (c) PCD(A) 'as-received' (600 m/min, 0.01 mm/z), (d) MS2050 'as-received' (60 m/min, 0.10 mm/z), and (e) Med. hone PCD(A) (450 m/min, 0.0134 mm/z). Higher magnification images of (a)–(e) are provided respectively in (i)–(v).

Table 4
Surface roughness metrics comparing surfaces generated with the PCD(A) and MS2050 tool grades.

Tool grade	V_c [m/min]	f_z [mm/z]	S_a [μm]	S_q [μm]	S_{sk} [μm]	S_{ku} [μm]
MS2050 (As-rec.)	60	0.1000	0.638	0.812	0.181	3.680
PCD(A) (As-rec.)	200	0.0300	0.646	0.821	0.169	3.391
PCD(A) (As-rec.)	450	0.0134	0.495	0.635	0.145	3.658
PCD(A) (As-rec.)	600	0.0100	0.477	0.625	0.085	3.986
PCD(A) (r_0 = Med.)	450	0.0134	0.592	0.769	0.179	3.977

The effect of cutting edge hone applied to the PCD tooling is shown by Fig. 18e. Comparisons to the subsurface condition following machining with the sharp tool as similar cutting parameters shows that the increased cutting edge radii has contributed to higher levels of SPD which can also be attributed to the ploughing mechanism.

Topographical surface roughness metrics associated with the surfaces generated for the metallurgical assessment are provided in Table 4. The PCD tooling and high speed/low feed rate machining strategy show capabilities at generating a higher surface finish quality with a reduction in arithmetic, S_a and root mean square S_q height distribution. Additionally, skewness S_{sk} is reduced suggesting a reduction in asperity heights associated with feed marks on the machined surface. Negligible differences in kurtosis S_{ku} were observed. The improvements

in surface roughness when machining with the PCD vs. the WC–Co tooling as well as the improvements during PCD machining when employing the high speed/low feed rate machining strategy can be attributed to a reduction in feed rate. The assessment of the surface machined with the honed PCD tooling also highlights that the sharp cutting edge is also advantageous in achieving a higher surface finish quality.

The results from the surface integrity assessment show promising findings for the use of PCD tooling and high cutting speed/low feed rate machining strategies for titanium alloy finishing applications. Whereas from a tool life standpoint, the negligible performance improvement would make it difficult to justify the use of PCD, in finishing applications where manufacturers seek to generate surfaces which display metallurgical properties which are unaltered from the bulk material, PCD may offer an effective alternative to WC–Co tooling.

4. Conclusions

This study has compared the performance of PCD and WC–Co tooling in a square shoulder milling application of Ti-54M. The influence of PCD grain size, cutting edge radii, and cutting parameter selection on tool life, cutting forces, and workpiece material response have been investigated. The main conclusions which can be drawn from this research are as follows:

1. At a similar MRR, PCD tooling demonstrated comparable flank wear resistance properties compared to WC–Co tools up to a total cutting time of 20 min. WC–Co tooling however, offered a longer overall tool life compared to PCD, due to its better wear resistance in the later stages of the life of the tool.
2. Mechanical fracture of the cutting edge was shown to be the predominant wear mechanisms for the PCD tooling at lower cutting speeds with a transition to an adhesive driven mechanism at higher cutting speeds. This mechanism exhibited adhesion of the workpiece material to the cutting edge followed by its subsequent removal, resulting in pull out of PCD grains from the Co binder matrix. This type of wear is typically referred to as spalling and in the present study was initiated when a cutting speed of 450 m/min and feed rate of 0.0134 mm/z was reached. Increasing the cutting speed and simultaneously reducing the feed rate beyond this was shown to increase spalling driven wear.
3. Optimum tool life for the PCD tooling was achieved at cutting parameters of 450 m/min, 0.0134 mm/z, corresponding to the point where the predominant tool degradation mechanism shifted from mechanical fracture to spalling.
4. The cutting force response during PCD machining shows a reduction in peak cutting forces as cutting parameters transition from high feed/low speed to low feed/high speed conditions.
5. This reduction in cutting forces was shown to improve PCD tool life in the chipping dominated wear regime (200–400 m/min).
6. A fine PCD grain size demonstrated superior tool life in this application. This was attributed to the higher fracture toughness associated with this grade.
7. Increasing the cutting edge radius of the PCD tooling was shown to have an adverse effect on tool life, with increased cutting edge radii yielding higher cutting forces and an increased tendency for cutting edge fracture.
8. When employing cutting parameters which prolong tool life, it has been demonstrated that cutting forces can be significantly reduced when machining with PCD tooling at high cutting speed/low feed rate cutting parameters compared to WC–Co tooling at conventional parameters. This has resulted in a workpiece material response which displays significantly lower levels of microstructural damage when machining with PCD tooling, which was attributed to a considerably lower ploughing cutting force component due to the sharp cutting edge radii and low feed rate.

It is important to emphasise that findings made in this study are based on the specific cutting application and insert geometry used. Alterations to these parameters may lead to cutting conditions where the wear mechanisms observed in the present work are less dominant and, under such circumstances, other PCD grain sizes may offer superior tool life. Future studies on PCD tool performance in milling applications should explore up milling strategies to determine their effects on tool wear mechanisms and possible benefits on tool life.

Declaration of competing interest

The authors declare that they have no known competing financial interests or personal relationships that could have appeared to influence the work reported in this paper.

Acknowledgements

This study was funded by the EPSRC, UK Industrial Doctorate Centre in Machining Science (EP/L016257/1) as well as Seco Tools and Element Six. The authors would like to acknowledge TIMET UK Ltd. for the supply of the Timetal® 54M.

References

[1] E.O. Ezugwu, Z. Wang, Titanium alloys and their machinability - a review, J. Mater Process. Technol. 68 (1997) 262–274, http://dx.doi.org/10.1016/B978-0-12-801238-3.99864-7.
[2] R. M'Saoubi, D. Axinte, S.L. Soo, C. Nobel, H. Attia, G. Kappmeyer, S. Engin, W.M. Sim, High performance cutting of advanced aerospace alloys and composite materials, CIRP Ann. - Manuf. Technol. 64 (2) (2015) 557–580, http://dx.doi.org/10.1016/j.cirp.2015.05.002.
[3] G.A. Oosthuizen, G. Akdogan, The performance of PCD tools in high-speed milling of Ti6Al4V, Int. J. Adv. Manuf. Technol. 52 (2011) 929–935, http://dx.doi.org/10.1007/s00170-010-2804-2.
[4] O. Hatt, Z. Lomas, M. Thomas, M. Jackson, The effect of titanium alloy chemistry on machining induced tool crater wear characteristics, Wear 408–409 (February) (2018) 200–207, http://dx.doi.org/10.1016/j.wear.2018.05.020.
[5] X. Liang, Z. Liu, Tool wear behaviors and corresponding machined surface topography during high-speed machining of Ti-6Al-4V with fine grain tools, Tribol. Int. 121 (February) (2018) 321–332, http://dx.doi.org/10.1016/j.triboint.2018.01.057.
[6] V. Calatoru, M. Balazinski, J. Mayer, H. Paris, G. L'Espérance, Diffusion wear mechanism during high-speed machining of 7475-T7351 aluminum alloy with carbide end mills, Wear 265 (11) (2008) 1793–1800, http://dx.doi.org/10.1016/j.wear.2008.04.052.
[7] M.H. Ali, R. Balasubramanian, B. Mohamed, B.A. Khidhir, Effects of coolants on improving machining parameters while machinability Titanium alloy (Ti-6Al-4V): A review, Appl. Mech. Mater. 110–116 (2012) 1657–1666, http://dx.doi.org/10.4028/www.scientific.net/AMM.110-116.1657.
[8] Y. Ayed, G. Germain, High-pressure water-jet-assisted machining of Ti555-3 titanium alloy : investigation of tool wear mechanisms, Int. J. Adv. Manuf. Technol. 96 (2018) 845–856, http://dx.doi.org/10.1007/s00170-018-1661-2.
[9] B. Dilip Jerold, M. Pradeep Kumar, The influence of cryogenic coolants in machining of Ti-6Al-4V, Trans. ASME, J. Manuf. Sci. Eng. 135 (3) (2013) 1–8, http://dx.doi.org/10.1115/1.4024058.
[10] A. Shokrani, V. Dhokia, S.T. Newman, Investigation of the effects of cryogenic machining on surface integrity in CNC end milling of Ti-6Al-4V titanium alloy, J. Manuf. Process. 21 (2016) 172–179, http://dx.doi.org/10.1016/j.jmapro.2015.12.002.
[11] A. Ugarte, R. M'Saoubi, A. Garay, P.J. Arrazola, Machining behaviour of Ti-6Al-4V and Ti-5553 alloys in interrupted cutting with PVD coated cemented carbide, Proc. CIRP 1 (1) (2012) 202–207, http://dx.doi.org/10.1016/j.procir.2012.04.035.
[12] R. Izamshah, R. Abdullah, B.I. Redzuwan, M. Sanusi, A. Aziz, M.S. Kasim, Comparative study of tool wear in milling titanium alloy (Ti-6Al-4V) using PVD and CVD coated cutting tool, Ind. Lubr. Tribol. 3 (October 2016) (2017) 363–370, http://dx.doi.org/10.1108/ILT-09-2016-0202.
[13] C.F. Wyen, K. Wegener, Influence of cutting edge radius on cutting forces in machining titanium, CIRP Ann. - Manuf. Technol. 59 (1) (2010) 93–96, http://dx.doi.org/10.1016/j.cirp.2010.03.056.
[14] Cutting edge geometry effect on plastic deformation of titanium alloy, IOP Conf. Ser.: Mater. Sci. Eng. 125 (1) (2016) http://dx.doi.org/10.1088/1757-899X/125/1/012012.
[15] A.C. Araujo, G. Fromentin, P. Blandenet, Investigation on PCD cutting edge geometry for Ti6Al4V high-feed milling, Int. J. Adv. Manuf. Technol. 111 (2020) 1785–1796, http://dx.doi.org/10.1007/s00170-020-06086-z.

[16] A. Saini, B.S. Pabla, S.S. Dhami, Developments in cutting tool technology in improving machinability of Ti6Al4V alloy: A review, Proc. Inst. Mech. Eng. B 230 (11) (2016) 1977–1989, http://dx.doi.org/10.1177/0954405416640176.
[17] A.K.M.N. Amin, A.F. Ismail, M.K.N. Khairusshima, Effectiveness of uncoated WC – Co and PCD inserts in end milling of titanium alloy - Ti-6Al-4V, J. Mater Process. Technol. 193 (2007) 147–158, http://dx.doi.org/10.1016/j.jmatprotec.2007.04.095.
[18] Z. Ren, S. Qu, Y. Zhang, F. Sun, X. Li, C. Yang, Machining performance of PCD and PCBN tools in dry turning titanium, Int. J. Adv. Manuf. Technol. 102 (2019) 2649–2661, http://dx.doi.org/10.1007/s00170-018-3074-7.
[19] S.U. Honghua, L.I.U. Peng, F.U. Yucan, X.U. Jiuhua, Tool life and surface integrity in high-speed milling of titanium alloy TA15 with PCD / PCBN tools, Chin. J. Aeronaut. 25 (5) (2012) 784–790, http://dx.doi.org/10.1016/S1000-9361(11)60445-7.
[20] G.D. Revankar, R. Shetty, S.S. Rao, V.N. Gaitonde, Analysis of surface roughness and hardness in titanium alloy machining with polycrystalline diamond tool under different lubricating modes, Mater. Res. 17 (4) (2014) 1010–1022, http://dx.doi.org/10.1590/1516-1439.265114.
[21] S. Sheikh, R.M. Saoubi, P. Flasar, M. Schwind, T. Persson, J. Yang, L. Llanes, Fracture toughness of cemented carbides : Testing method and microstructural effects, Int. J. Refract. Met. Hard Mater. (2014) URL http://dx.doi.org/10.1016/j.ijrmhm.2014.08.018.
[22] Hardness to toughness relationship of fine-grained WC-Co hardmetals, Int. J. Refract. Met. Hard Mater. 16 (2) (1998) 133–142, http://dx.doi.org/10.1016/S0263-4368(98)00028-6.
[23] V.F.C. Sousa, F. Jos, D. Silva, G.F. Pinto, A. Baptista, R. Alexandre, Characteristics and wear mechanisms of tialn-based coatings for machining applications : A comprehensive review, Metals 11 (2021) 260, URL https://doi.org/10.3390/met11020260.
[24] G. Li, S. Yi, S. Sun, S. Ding, Wear mechanisms and performance of abrasively ground polycrystalline diamond tools of different diamond grains in machining titanium alloy, J. Manuf. Process. 29 (2017) 320–331, http://dx.doi.org/10.1016/j.jmapro.2017.08.010.
[25] C.J. Pretorius, S.L. Soo, D.K. Aspinwall, P.M. Harden, R. M'Saoubi, A.L. Mantle, Tool wear behaviour and workpiece surface integrity when turning Ti-6Al-2Sn-4Zr-6Mo with polycrystalline diamond tooling, CIRP Annals 64 (1) (2015) 109–112, http://dx.doi.org/10.1016/j.cirp.2015.04.058.
[26] A. Jawaid, S. Sharif, S. Koksal, Evaluation of wear mechanisms of coated carbide tools when face milling titanium alloy, J. Mater Process. Technol. 99 (2000) 266–274, http://dx.doi.org/10.1016/S0924-0136(99)00438-0.
[27] R. Lindvall, F. Lenrick, H. Persson, R.M. Saoubi, J.-e. Ståhl, Performance and wear mechanisms of PCD and pcBN cutting tools during machining titanium alloy Ti6Al4V, Wear 454–455 (2020) 203329, http://dx.doi.org/10.1016/j.wear.2020.203329.
[28] G. Li, N. Li, C. Wen, S. Ding, Investigation and modeling of flank wear process of different PCD tools in cutting titanium alloy Ti6Al4V, Int. J. Adv. Manuf. Technol. 95 (2018) 719–733, http://dx.doi.org/10.1007/s00170-017-1222-0.
[29] S. Husain, I. Jaffery, M. Khan, N. Sheikh, P. Mativenga, Wear mechanism analysis in milling of Ti-6Al-4V alloy, Proc. IMechE Part B: J. Eng. Manuf. 227 (8) (2013) 1148–1156, http://dx.doi.org/10.1177/0954405413481210.
[30] A. Li, J. Zhao, D. Wang, J. Zhao, Failure mechanisms of a PCD tool in high-speed face milling of Ti-6Al-4V alloy, Int. J. Adv. Manuf. Technol. 67 (2013) 1959–1966, http://dx.doi.org/10.1007/s00170-012-4622-1.
[31] V. Venkatesh, Y. Kosaka, J. Fanning, S. Nyakana, Processing and properties of timetal 54M, Ti-2007 Sci. Technol. Jpn. Inst. Met. (2007) 713–716.
[32] M. Armendia, A. Garay, L. Iriarte, P. Arrazola, Journal of materials processing technology comparison of the machinabilities of Ti6Al4V and TIMETAL® 54M using uncoated WC – Co tools, J. Mater Process. Technol. 210 (2010) 197–203, http://dx.doi.org/10.1016/j.jmatprotec.2009.08.026.
[33] S. Zhang, J.F. Li, J. Sun, F. Jiang, Tool wear and cutting forces variation in high-speed end-milling Ti-6Al-4V alloy, Int. J. Adv. Manuf. Technol. 46 (2010) 69–78, http://dx.doi.org/10.1007/s00170-009-2077-9.
[34] B. Rosemar, Á.R. Machado, E.O. Ezugwu, J. Bonney, W.F. Sales, Journal of materials processing technology tool life and wear mechanisms in high speed machining of Ti – 6Al – 4V alloy with PCD tools under various coolant pressures, J. Mater Process. Technol. 213 (8) (2013) 1459–1464, http://dx.doi.org/10.1016/j.jmatprotec.2013.03.008.
[35] M. Brown, R. M'Saoubi, P. Crawforth, A. Mantle, J. McGourlay, H. Ghadbeigi, On deformation characterisation of machined surfaces and machining-induced white layers in a milled titanium alloy, J. Mater Process. Technol. 299 (September 2021) (2022) 117378, URL https://doi.org/10.1016/j.jmatprotec.2021.117378.
[36] T.L. Ginta, M.A. Lajis, U. Tun, H. Onn, A.N. Amin, The performance of uncoated tungsten carbide insert in end milling titanium alloy Ti-6Al 4V through work piece preheating, Am. J. Eng. Appl. Sci. 2 (1) (2009) 147–153.
[37] C.R. Dandekar, Y.C. Shin, J. Barnes, Machinability improvement of titanium alloy (Ti-6Al-4V) via LAM and hybrid machining, Int. J. Mach. Tools Manuf. 50 (2) (2010) 174–182, http://dx.doi.org/10.1016/j.ijmachtools.2009.10.013.
[38] C. Veiga, J.P. Davim, A.J. Loureiro, Review on machinability of titanium alloys: The process perspective, Rev. Adv. Mater. Sci. 34 (2) (2013) 148–164.
[39] M. Brown, P. Crawforth, R. M'Saoubi, T. Larsson, B. Wynne, A. Mantle, H. Ghadbeigi, Quantitative characterization of machining-induced white layers in Ti–6Al–4V, Mater. Sci. Eng. A 764 (July) (2019) 138220, http://dx.doi.org/10.1016/j.msea.2019.138220.
[40] P. Crawforth, Towards a Micromechanistic Understanding of Imparted Subsurface Deformation During Machining of Titanium Alloys (Ph.D. thesis), The University of Sheffield, 2014, pp. 146–151, URL https://etheses.whiterose.ac.uk/7155/1/PeteCrawforthThesis-Doublesidedprinting.pdf.